JOURNAL OF SPACECRAFT AND ROCKETS
Vol. 29, No. 2, March–April 1992

Comparison of Heating Calculations with Experimental Data on a Modified Shuttle Orbiter

H. Harris Hamilton II,* Francis A. Greene,† and K. James Weilmuenster‡
NASA Langley Research Center, Hampton, Virginia 23665

Heating-rate calculations from an "engineering" code and a "benchmark" Navier-Stokes code are compared with experimental wind-tunnel data obtained on a "modified" 0.0075 scale Shuttle Orbiter at a Mach number of 6 and a freestream Reynolds number of 1.9×10^6/m. Comparisons are presented along the windward symmetry plane, in a circumferential direction around the body, and along the wing leading edge at angles of attack of 30 and 40 deg. From these results, it is shown that both codes provide accurate predictions of the heating rate over most of the body, but because the run time for the engineering code is relatively short, it is an ideal tool for both parametric and design studies.

Nomenclature

h	= metric coefficient (see Fig. 2)
L	= vehicle length
M	= Mach number
p	= static pressure
q	= surface heating rate
Re	= Reynolds number
r, ϕ, z	= cylindrical coordinates
s	= surface distance measured normal to windward symmetry plane
s, β, n	= streamline coordinates (see Fig. 2)
T	= static temperature
x, y, z	= Cartesian coordinates (see Fig. 1)
α	= angle of attack
γ	= ratio of specific heats

Subscripts

b	= body
w	= wall
∞	= freestream

Introduction

THE calculation of aerodynamic heating on advanced entry vehicles is a challenging problem. Configurations of current interest are usually three-dimensional bodies (see Fig. 1) that can operate at large angles of attack during periods of peak heating. Since ground-based experimental facilities cannot simulate the real-gas environment of flight, it is necessary to rely heavily on computational fluid dynamic (CFD) flowfield codes to predict the flight environment.

To design these vehicles, it is necessary to have both engineering and benchmark computer codes that can be used to predict the aerothermodynamic environment of flight. The engineering codes use approximate numerical methods and descriptions of physical phenomena and are designed to provide reasonably accurate results and run very rapidly on today's computers. They can be used to perform the parametric studies required for system design. The benchmark codes use the best available numerical techniques and descriptions of physical phenomena and provide detailed flowfield predictions for both the forebody and wake regions of the vehicle. These codes can be used to provide detailed information about the flowfield; but with today's computers, their run times can be very large (i.e., several hours for a complex vehicle such as the Shuttle Orbiter).

Before these computer codes are applied to vehicle design, they should first be validated by comparing them with experimental data at wind-tunnel conditions and then by similar comparisons at flight conditions. However, in most cases, flight data at the relevant flight conditions are not available. Thus, it is often necessary first to validate benchmark codes at wind-tunnel conditions and then to use these benchmark codes to calibrate engineering codes for the real-gas environment of flight.

In the case of the Shuttle Orbiter, both wind-tunnel[1] and flight[2] data are available, but the number of measuring locations (especially off the symmetry plane) was severely limited. Although code verification studies have been undertaken previously,[3] the scope of these studies has been restricted, especially off the symmetry plane in the vicinity of wing leading edges where the data are sparse. In response to this need, a new wind-tunnel heat-transfer model[4] has been built using "thin film" gauge technology that provides a much more detailed distribution of heating-rate measurements off the symmetry plane and provides results designed specifically for code verification studies. This model has been tested in the Langley 20-in. Mach 6 tunnel.

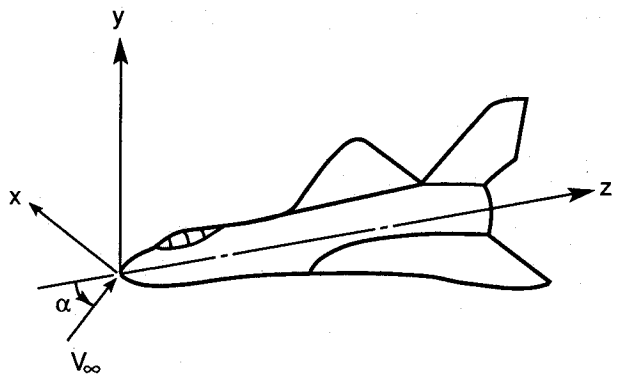

Fig. 1 Typical advanced re-entry vehicle.

Received June 3, 1991; presented as Paper 91-1347 at the AIAA 26th Thermophysics Conference, Honolulu, HI, June 24–26, 1991; revision received Oct. 9, 1991; accepted for publication Oct. 10, 1991.

*Research Leader, Aerothermodynamics Branch, Space Systems Division. Senior Member AIAA.
†Aerospace Technologist, Aerothermodynamics Branch, Space Systems Division. Member AIAA.
‡Senior Research Engineer, Aerothermodynamics Branch, Space Systems Division. Senior Member AIAA.

The purpose of the present paper is to compare heating-rate calculations from an engineering code (AA3DBL[3]) with those obtained from a benchmark Navier-Stokes code (LAURA[5]) and with experimental data[4] obtained at Mach 6 in air. Comparisons will be presented at angles of attack of 30 and 40 deg for Reynolds numbers of 1.9×10^6/m. This will provide more detailed information about the ability of these codes to predict the heating in the vicinity of wing leading edges where the heating rates are expected to be very high.

Computational Methods

In the present paper, heating-rate calculations from an engineering code (AA3DBL) and similar results from a benchmark Navier-Stokes code (LAURA) are compared with experimental data measured on a modified Shuttle Orbiter in the Langley 20-in. Mach 6 tunnel. Brief descriptions of the computer codes are presented in this section.

AA3DBL

The AA3DBL code is an approximate three-dimensional heating code based on the axisymmetric analog for three-dimensional boundary layers, and the details of its development are given in Ref. 3. In this method, the general three-dimensional boundary-layer equations are first written in a streamline-oriented coordinate system (s, β, n) where s is measured along an inviscid surface streamline, β is tangent to the surface and normal to the streamline direction, and n is normal to the surface (see Fig. 2). If the crossflow velocity in the boundary layer is small and can be neglected, the boundary-layer equations reduce to the same form as for axisymmetric flow, provided that s is interpreted as distance along an "equivalent" axisymmetric body and the metric h, associated with the spreading of streamlines, is interpreted as the radius of the equivalent axisymmetric body. This greatly simplifies the boundary-layer problem and means that approximate three-dimensional heating rates can be computed along individual streamlines independent of other streamlines using any axisymmetric method. It has been shown that the assumption of small crossflow in the boundary layer is valid[3] when the streamline curvature is small or when the wall is highly cooled (as it is in many hypersonic applications). To apply this method, the inviscid surface streamlines and metric coefficients are required. Although several approaches have been used, it has been found that the best approach is to use inviscid velocity components obtained from a three-dimensional inviscid flowfield solution.[3] In the present paper, velocity components calculated by the HALIS[6] code are used to provide this information and also to provide edge conditions for the boundary-layer calculations. Approximate heating relations developed by Zoby et al.[7] have been used to calculate the surface heating rate.

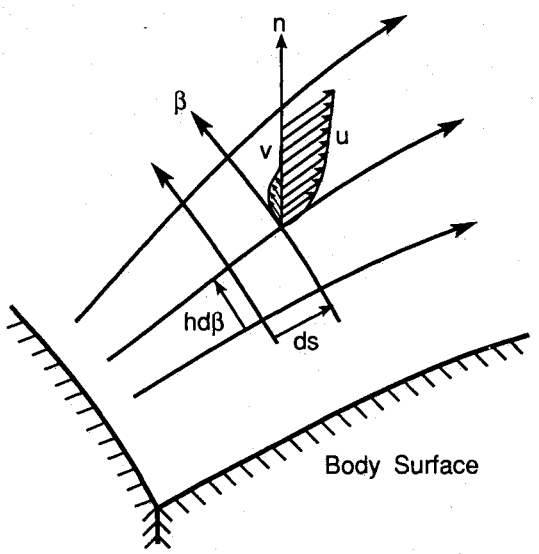

Fig. 2 Typical streamlines and boundary-layer velocity profile.

Table 1 Solution times

Code	Grid	Time, h	Computer
HALIS	15 × 73 × 145	0.8	Cray-YMP
LAURA	70 × 81 × 145	50.0	Cray-2
LAURA	81 × 81 × 145	60.0	Cray-2
AA3DBL	145	0.2	Sun SPARC 2

The approach used to track streamlines has been modified since the publication of Ref. 3. In that paper, a streamline was chosen and then followed from its origin at the stagnation point until it reached the end of the body. Then another streamline was chosen and followed from the stagnation point to the end of the body. In principle, proceeding in this fashion, the heating rate on the entire body surface could be calculated. However, in practice this approach was very time consuming to apply because the path that a given streamline would trace out on the body was not known a priori. Large regions of the body (particularly on a wing) were often missed entirely on the first pass, and it became a very laborious task to repeat the process of selecting streamlines (usually requiring several passes) until the heating on the entire body was adequately defined. To circumvent this problem, the streamline computing procedure has been modified. The new procedure involves selecting a reasonably large number of streamlines that are all computed simultaneously from the stagnation point; then, at each new computational step down the body the streamlines are redistributed to achieve a more uniform distribution around the body. Thus, the heating over the entire body can be computed in a single pass with no user intervention. This new procedure greatly reduces the overall time required to complete a solution.

For all of the cases presented in the present paper, 145 streamlines are used to march the solution downstream. The computing time for AA3DBL is shown in Table 1; however, it should be noted that the time required to obtain an inviscid solution should be added to this to obtain the true computational time for a given case.

HALIS

The HALIS inviscid flowfield code was initially developed to handle the high-angle-of-attack flowfields about the Shuttle Orbiter, which were characterized by large regions of embedded subsonic flow on the windward surface. The HALIS code is described in detail in Ref. 6. Briefly, the code is a time-asymptotic solution of the Euler equations that utilizes an unsplit MacCormack differencing scheme. The solution space is the volume between the body surface and the bow-shock wave, which is treated as a time-dependent boundary. This leads to a coordinate system defined by the position of the bow shock and the body, as well as the spatial derivatives along these surfaces. The HALIS code uses a spherical coordinate system to describe the nose region of a vehicle and is matched to a cylindrical coordinate system that describes the rest of the vehicle. For vehicles that can be described in this coordinate system, it offers an efficient method for computing the inviscid flowfield solution. In the present paper, the cases presented were computed with a grid of 15 points between the body and shock, 73 points around the body, and 145 planes down the body. The approximate computing time for HALIS for these cases is shown in Table 1.

LAURA

The formulation of the Langley Aerothermodynamic Upwind Relaxation Algorithm (LAURA) is presented in detail in Ref. 5. The version of the LAURA code used in the present

paper is a three-dimensional finite volume algorithm that solves the thin-layer Navier-Stokes equations for laminar perfect-gas flows. Inviscid fluxes are either first- or second-order accurate. A first-order flux is constructed using Roe's flux difference splitting,[8] and symmetric total variation diminishing (STVD)[9] differencing is used to compute second-order fluxes. Viscous terms are approximated using second-order central differences.

The governing equations are relaxed in pseudotime until the solution reaches steady state. The treatment of the governing equations is described as point implicit because variables at the cell center of interest are treated implicitly, whereas the latest available data are used for the left-hand-side numerics. With this strategy, updating cell-centered variables requires the inversion of only a 5×5 matrix and only one level of storage. Specific information regarding the perfect-gas formulation, boundary conditions, and the Jacobians is contained in Ref. 5.

In the present paper, the results for $\alpha = 30$ deg were computed with a grid of 70 points between the body and outer boundary, 81 points around the body, and 145 planes down the body. For $\alpha = 40$ deg, the number of grid points between the body and outer boundary was increased to 81 and the remainder of the grid remained the same as for the $\alpha = 30$ deg case. The approximate computing times for these two cases are shown in Table 1. It should be noted that no attempt has been made to optimize the computational time for the LAURA code, and with further work in this area significant improvements may be possible.

Geometry Description

The vehicle configuration used for making flowfield calculations in the present paper is modeled with QUICK, a geometry description program described in Ref. 10. This model provides a smooth piecewise analytic description of the vehicle geometry in a "local polar coordinate system," $r_b = r_b(z, \phi)$, with continuous surface derivatives over the vehicle.

Two versions of the geometry of the Space Shuttle Orbiter (shown in Fig. 3) have been modeled with QUICK as shown in Fig. 4. The first (Fig. 4a) is a reasonably accurate model of the actual vehicle geometry with the vertical tail removed. The second (Fig. 4b) has the same lower surface shape and the same profile (except for the canopy) for the upper surface symmetry plane as the first but has been "modified" by filling in the region between the leading edge of the strake or wing and the upper symmetry plane with elliptical segments as shown by the dashed lines in section A-A of Fig. 3. This process simplifies the leeside geometry and makes calculations in this region easier but does not affect the results obtained on the windward side because the crossflow velocity component goes supersonic near the leading edge of the strake or wing.

Experimental Data

In previous heat transfer tests on vehicles such as the Shuttle Orbiter, most instrumentation has been concentrated on the windward or leeward symmetry planes, with limited measurements in a circumferential or lateral direction away from the symmetry planes. To correct this problem, a 0.0075 scale model has been designed and tested at the Langley Research Center (see Ref. 4), which provides a large number of heat transfer measurements on the windward side of the body with most of the instrumentation located off of the symmetry plane. Since this model has a reasonably good distribution of gauges in the wing leading-edge region, it provides much needed data for CFD code verification. To ensure that the geometry of the model is well known and that the results can be used in a large number of CFD codes, the coordinates for the model were taken from the "modified" Shuttle Orbiter geometry described in the previous section. This model has been designated as the "HALIS Orbiter" since it was originally designed to be used with the HALIS inviscid code and the AA3DBL boundary-layer code for verification. The experimental heat transfer results presented in the present paper were obtained on this model. The freestream conditions for the experimental cases presented in the present paper are given in Table 2. A detailed description of these tests is presented in Ref. 4.

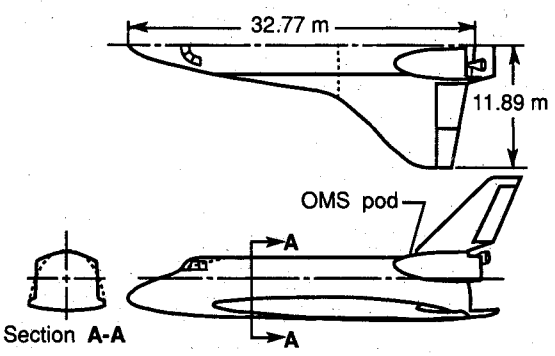

Fig. 3 Full-scale Space Shuttle Orbiter geometry.

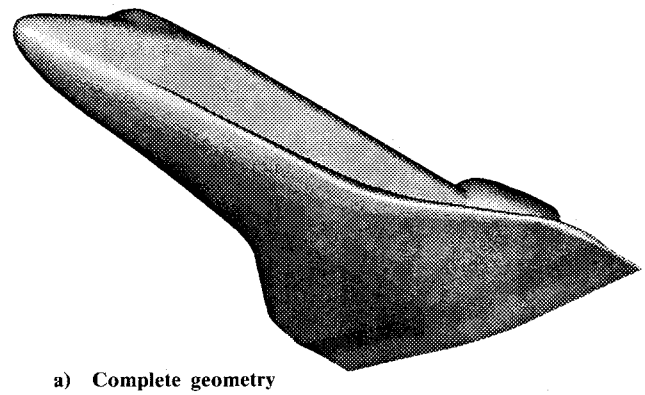

a) Complete geometry

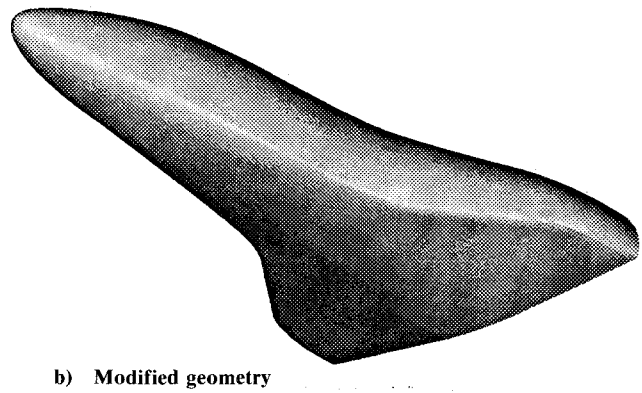

b) Modified geometry

Fig. 4 QUICK geometry models.

Table 2 Freestream flow conditions

Case	α, deg	p_∞, N/m^2	T_∞, K	M_∞	Re, m^{-1}
1	30	153.2	61.91	5.83	1.94×10^6
2	40	149.1	62.34	5.82	1.86×10^6

Results and Discussion

Heating rate calculations from AA3DBL and LAURA are compared with experimental data at $\alpha = 30$ deg in Figs. 5 and 6. The data were obtained in air ($\gamma = 1.4$) on a modified Shuttle Orbiter at a Mach number of 5.8. The freestream Reynolds number for the tests was approximately 1.9×10^6/m. For all of the results presented, the flow is laminar. The computational times and grids for this case are shown in Table 1. The heating results for AA3DBL shown in these figures are based on using 145 streamlines to march the solution down the body and using inviscid information and boundary-layer edge con-

ditions obtained from HALIS with a grid of 15 × 73 × 145. The heating results for LAURA for this case are based on solutions using a grid of 70 × 81 × 145. The wall temperature used in the computations was held constant at the average value measured during the experimental tests.

The comparison of heating rates along the windward symmetry plane is presented in Fig. 5. The results are plotted as q_w vs z/L, where z is the distance along the model axis measured from the nose. The LAURA results are slightly higher than the AA3DBL results over most of the forward part of the body ($z/L \leq 0.85$); but both agree with the experimental data within approximately ±10%. Further rearward on the body ($z/L > 0.85$), the LAURA results fall slightly below both the experimental data and the AA3DBL results. The grid resolution for LAURA in this region is thought to be insufficient to resolve the flow completely as it expands onto the rearward portion of the model's lower surface, which may account for the slight underprediction in this region. However, both calculations are still in reasonably good agreement with the data.

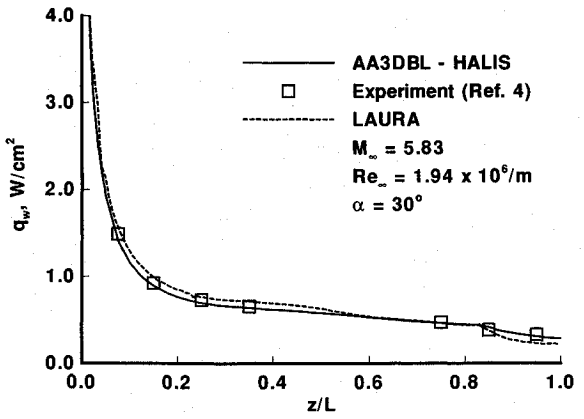

Fig. 5 Windward symmetry plane heating-rate distribution.

The comparison of heating rates in a circumferential direction around the model is presented in Fig. 6 at various stations along the model axis (i.e., constant values of z/L). The results are plotted as q_w vs s/L, where s is the surface distance around the model measured normal to the symmetry plane, starting on the lower surface and increasing toward the upper surface. In general, for each of the z/L stations, the heating first increases in a direction away from the symmetry plane, then reaches a peak near the leading edge, and finally decreases rapidly on the leeside. This behavior of the circumferential heating distribution can be better understood by referring to the circumferential pressure distribution at $z/L = 0.55$ shown in Fig. 7, which is typical of all cross-sectional stations, and to the streamline pattern shown in Fig. 8. Comparing the heating distribution shown in Fig. 6d with the pressure distribution shown in Fig. 7, it is seen that the heating rises as s/L increases, and there is an inflection point near $s/L = 0.075$ where the pressure reaches a maximum. Further outboard the pressure begins to decrease, slowly at first and then rapidly as the wing leading edge is approached. This causes the lateral component of velocity to accelerate as the leading edge is approached, which causes the streamlines in this region to diverge (see Fig. 8) and leads to the peak in heating near the leading edge. On the windward side of the body, the LAURA results are, in general, slightly higher than the AA3DBL results, but both agree reasonably well with the experimental data. On the leeward side of the body, the LAURA results are in slightly better agreement with the experimental data as should be expected because the flow in this region is viscous dominated and the AA3DBL results are based on an inviscid flowfield solution. The sharp increase in heating near the leading edge at stations $z/L = 0.65$ (Fig. 6e) and $z/L = 0.75$ (Fig. 6f) is probably the result of the formation of a shock near the wing leading edge and will be discussed in more detail later. For z/L stations of 0.55 and greater (Figs. 6d–6h), the peak values of heating near the leading edge predicted by LAURA are much higher than those predicted by AA3DBL. It should be noted that a sharp dip in the LAURA results (heating rate

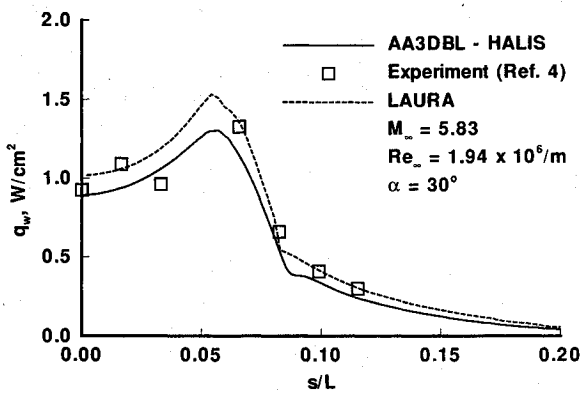

Fig. 6a Circumferential heating-rate distribution; $z/L = 0.15$.

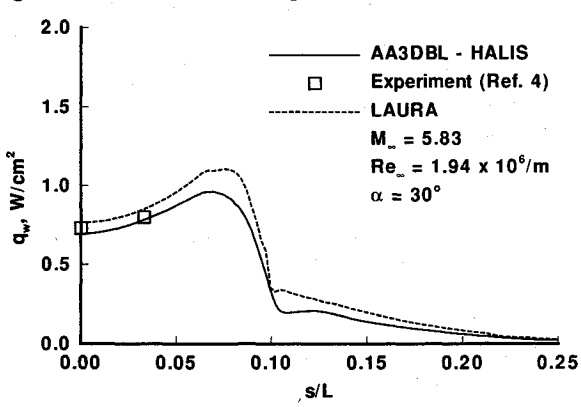

Fig. 6b Circumferential heating-rate distribution; $z/L = 0.25$.

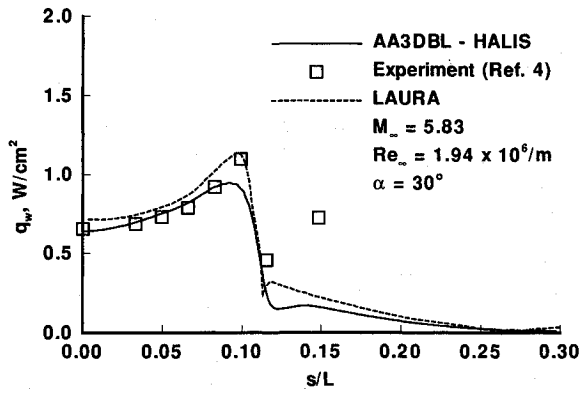

Fig. 6c Circumferential heating-rate distribution; $z/L = 0.35$.

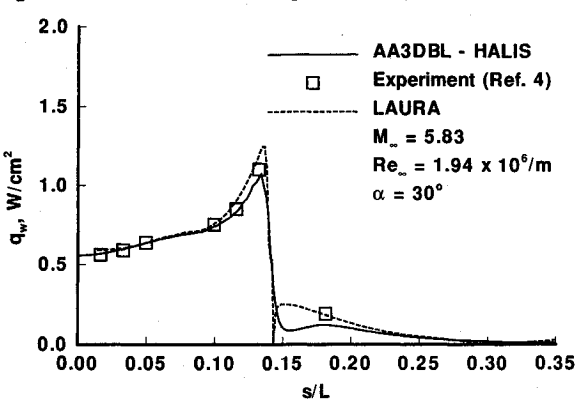

Fig. 6d Circumferential heating-rate distribution; $z/L = 0.55$.

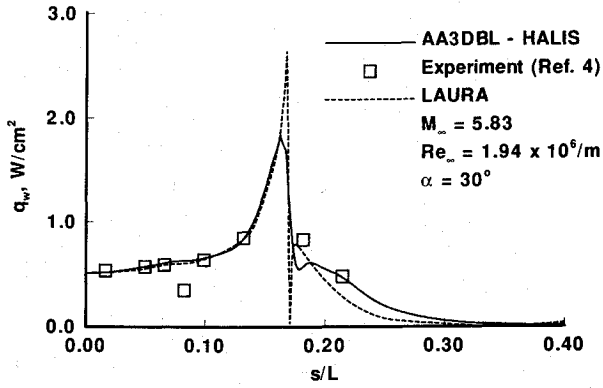

Fig. 6e Circumferential heating-rate distribution; $z/L = 0.65$.

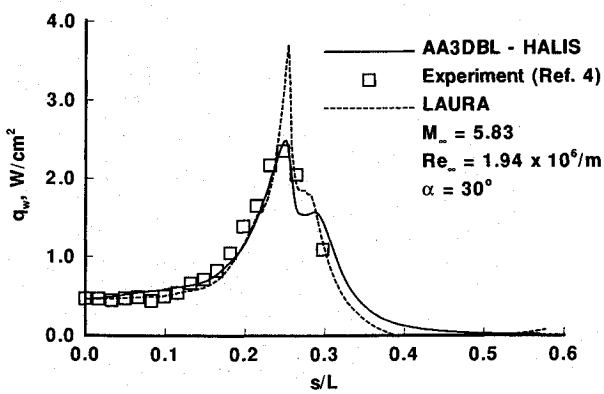

Fig. 6f Circumferential heating-rate distribution; $z/L = 0.75$.

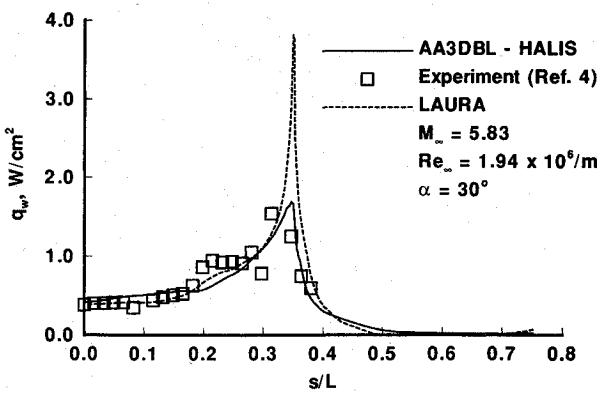

Fig. 6g Circumferential heating-rate distribution; $z/L = 0.85$.

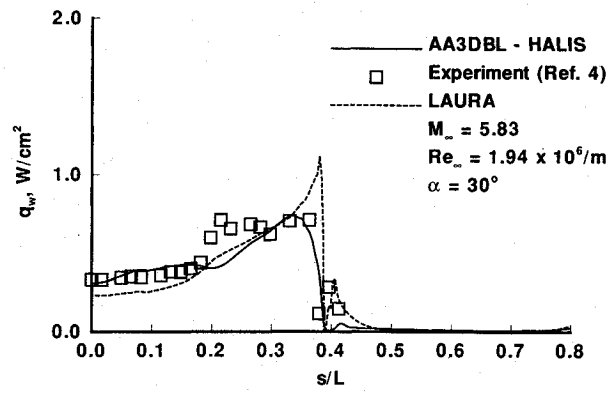

Fig. 6h Circumferential heating-rate distribution; $z/L = 0.95$.

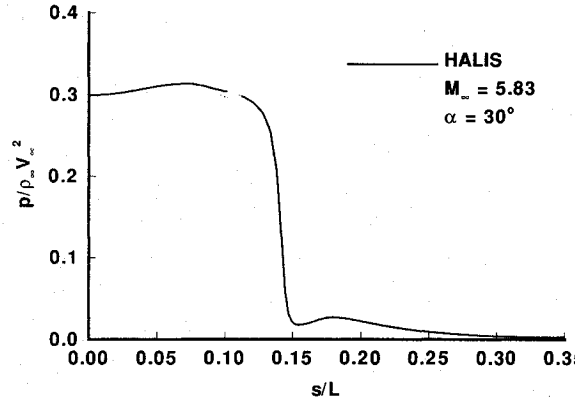

Fig. 7 Circumferential pressure distribution at $z/L = 0.55$.

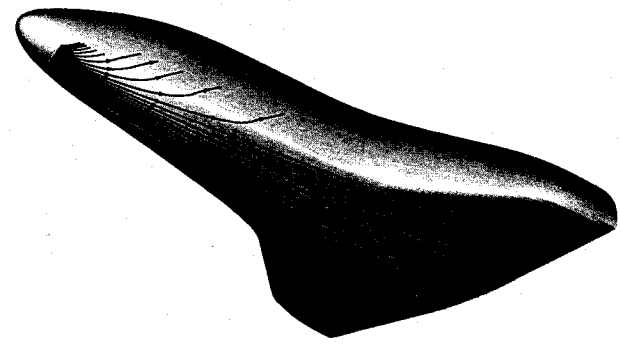

Fig. 8 Streamline pattern.

approaching zero) occurs just outboard of the wing leading edge for some z stations downstream of $z/L = 0.55$. This is thought to be due to a grid resolution problem in this region that probably also affects the peak heating calculations near the wing leading edge.

For the $z/L = 0.85$ and 0.95 stations (Figs. 6g and 6h) the experimental data rise to a plateau for $0.2 \leq s/L \leq 0.3$. Although these phenomena are underpredicted by both codes, the LAURA results exhibit a similar qualitative behavior and are in slightly better agreement with the data. Although the reason for this behavior is unknown, it may be the result of either a viscous or three-dimensional effect associated with the formation of the wing shock further upstream. However, except in this region and the leading-edge region on the aft portion of the lower surface, the heating rates predicted by both LAURA and AA3DBL are in reasonably good agreement with the experimental data.

The heating rates on the wing (or fuselage) leading edge for $\alpha = 30$ deg are presented in Fig. 9 as a function of z/L. The experimental values of heating are shown only for those cross sections where a gauge was located near the leading edge. It should be noted that the experimental measurements, although dense compared with previous experimental studies, may not be sufficiently dense to capture the "absolute maximum" leading-edge heating and thus the actual peak heating values could be higher than those shown. The rapid rise in heating near $z/L = 0.6$ is associated with the beginning of the wing. The maximum leading-edge heating rate occurs near $z/L = 0.7$ in the vicinity of the start of the wing shock, which is evident in the density contours shown in Fig. 10 (obtained from an inviscid LAURA solution). For both the experimental and AA3DBL results, the heating decreases rapidly immediately downstream of this point, levels out near the start of the bow-shock wing-shock intersection ($z/L = 0.75$) and then finally decreases rapidly as the wing turns more parallel to the flow ($z/L = 0.85$). As discussed previously, the LAURA code significantly overpredicts the measured heating rate in this region ($z/L \geq 0.75$) and is thought to be due to the grid used in the LAURA calculations. Because of these results, the LAURA grid was refined before the $\alpha = 40$ deg results were

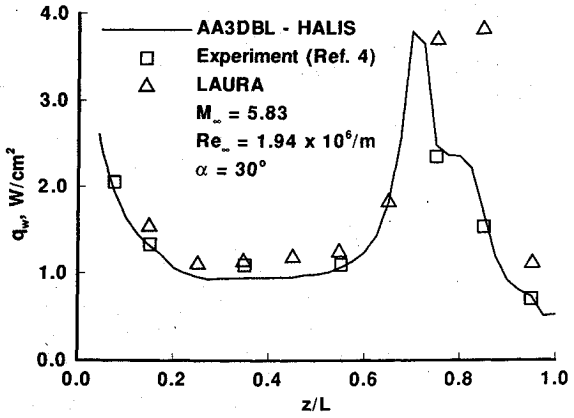

Fig. 9 Heating-rate distribution along leading edge.

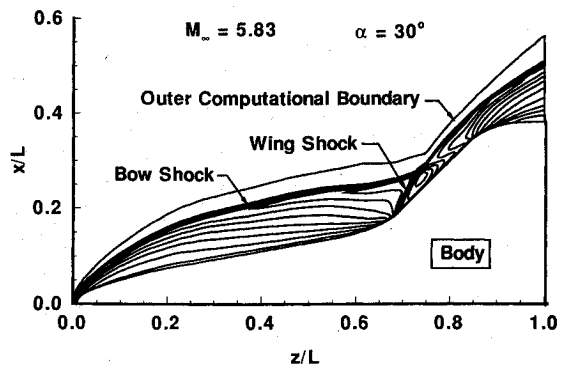

Fig. 10 Density contours in plane near leading edge.

computed and, as will be shown, the agreement with the experimental data in this region was greatly improved. The pressure distribution along the wing leading edge is shown in Fig. 11. The pressure follows a trend similar to that for the heating.

The computational time for this case (α = 30 deg) was approximately 50 h on a Cray-2 for LAURA and approximately 0.8 h on a Cray-YMP for AA3DBL/HALIS (actually 0.8 h on a Cray-YMP for HALIS and a few minutes on a Sun Workstation for AA3DBL). It should be noted, however, that the LAURA code used to perform the present calculations was not optimized to reduce run time and that significant improvements in run time could probably be achieved.

Heating rate calculations from AA3DBL and LAURA are compared with experimental data at α = 40 deg in Figs. 12 and 13. These data were obtained at the same freestream conditions as those previously discussed for α = 30 deg, and the flow is completely laminar. Before these calculations were performed, the grid used in the LAURA code was refined by adding additional grid points in the normal direction (see Table 1) and improving the grid distribution around the leading edges. This was done in an attempt to alleviate some of the problems discussed earlier for the α = 30 deg case that were thought to be associated with poor grid resolution.

The windward symmetry plane comparisons for this case are similar to those shown previously for α = 30 deg. The LAURA predictions are slightly higher than those from AA3DBL, but both are in reasonably good agreement with the experimental data (within approximately ±10%).

The comparison of heating rates in a circumferential direction around the body is presented in Fig. 13 at various stations along the body axis (i.e., constant values of z/L). The results are plotted as q_w vs s/L, where s is the surface distance around the model measured normal to the axis, starting at the windward symmetry plane. In general, the comparisons are similar to those presented previously for α = 30 deg in Fig. 6. The heating first increases in a direction away from the symmetry plane, then reaches a peak near the leading edge, and finally decreases rapidly on the leeside. It should be noted that for z/L = 0.85 and 0.95 (Figs. 13g and 13h) and $0.2 \le s/L \le 0.3$ the LAURA results are in much better agreement with the experimental data than for the previous case at α = 30 deg. This is probably the result of the improved grid used for this case. However, AA3DBL still underpredicts both the experimental data and the LAURA results in this region. This may be because of the existence of viscous effects or because of inadequate grid resolution for the HALIS inviscid flowfield calculations from which the streamlines and the boundary-layer edge conditions for AA3DBL were obtained. There is also some apparent scatter in the experimental heating data. However, for most of the remainder of the body the heating rates predicted by both LAURA and AA3DBL are in reasonably good agreement with the experimental data.

The heating rates on the wing (or fuselage) leading edge for this case are presented in Fig. 14 as a function of z/L. The experimental values of heating are shown only for those cross sections where a gauge was located near the leading edge. The results for this angle of attack are similar to those for α = 30 deg shown previously in Fig. 9. It should be remembered that the experimental values might be slightly higher if more gauges were located near the leading edge so that a better maximum could be defined. The rapid rise in heating near z/L = 0.6 is associated with the beginning of the wing. The maximum leading-edge heating rate (calculated by AA3DBL) occurs between z/L = 0.7 and 0.75. It was shown previously for α = 30 deg that the maximum leading-edge heating is associated with the start of the wing shock. Downstream of the region of maximum heating, the heating decreases, but not as rapidly as for α = 30 deg, and the LAURA results are in better agreement with the experimental data than are the AA3DBL results. The oscillations in the AA3DBL heating distributions near the end

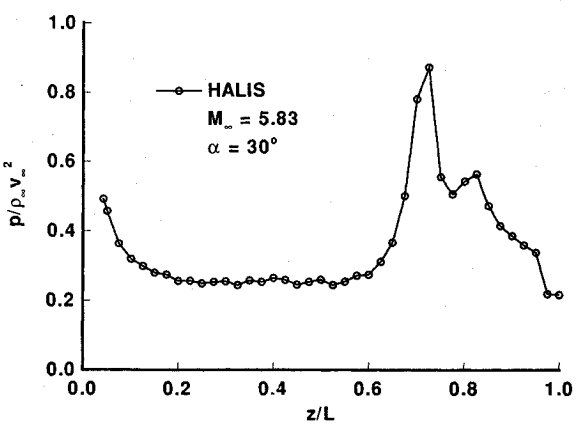

Fig. 11 Pressure distribution along leading edge.

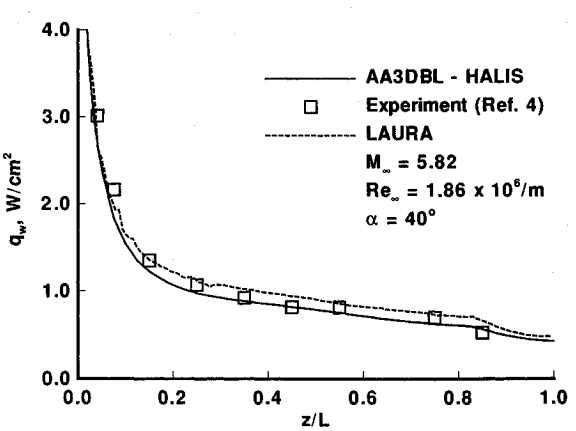

Fig. 12 Windward symmetry plane heating-rate distribution.

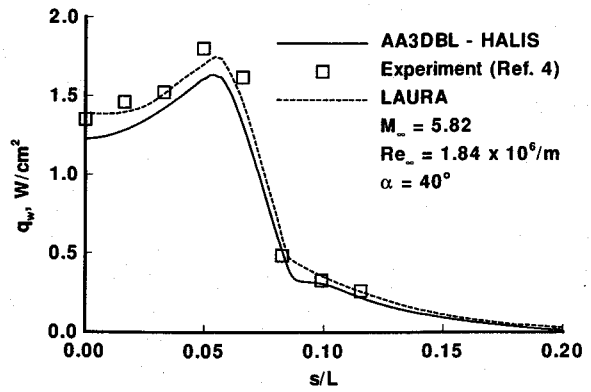

Fig. 13a Circumferential heating-rate distribution; $z/L = 0.15$.

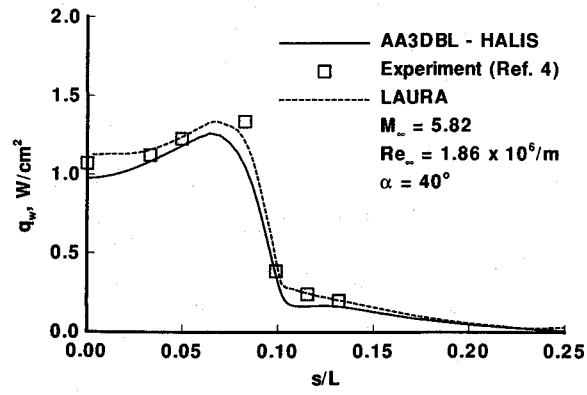

Fig. 13b Circumferential heating-rate distribution; $z/L = 0.25$.

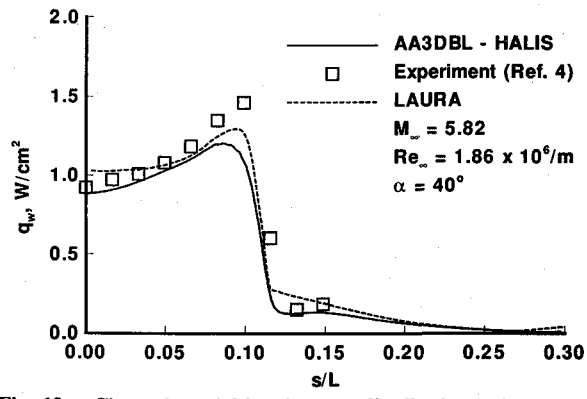

Fig. 13c Circumferential heating-rate distribution; $z/L = 0.35$.

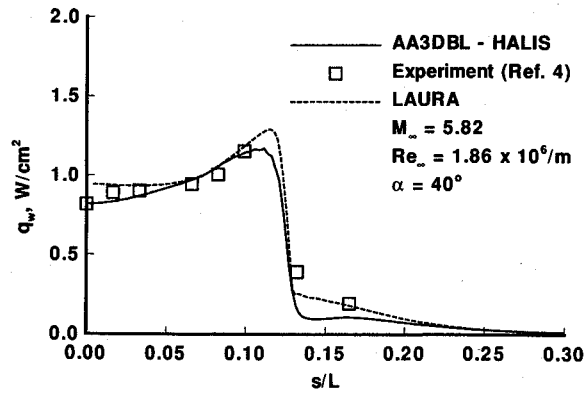

Fig. 13d Circumferential heating-rate distribution; $z/L = 0.45$.

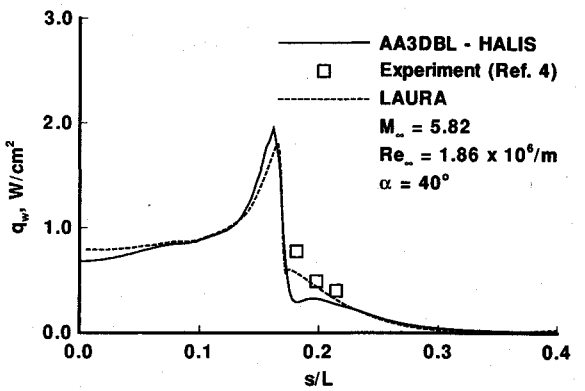

Fig. 13e Circumferential heating-rate distribution; $z/L = 0.65$.

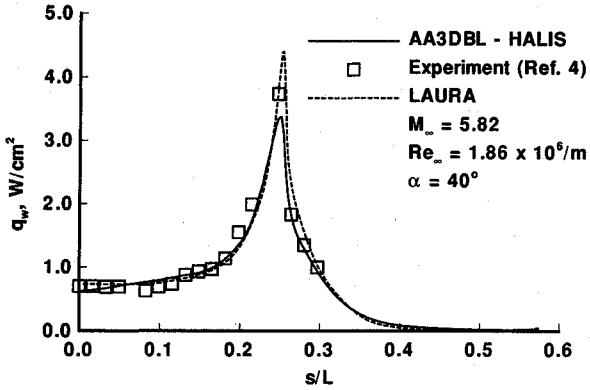

Fig. 13f Circumferential heating-rate distribution; $z/L = 0.75$.

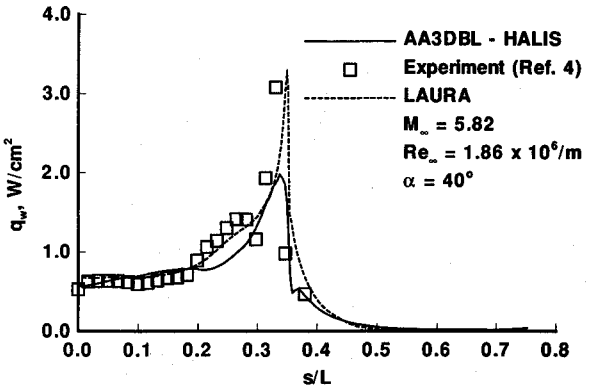

Fig. 13g Circumferential heating-rate distribution; $z/L = 0.85$.

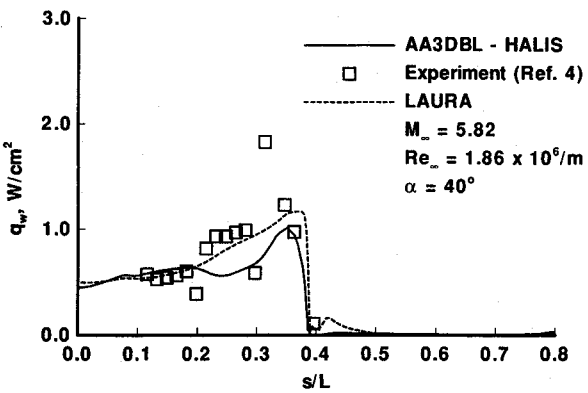

Fig. 13h Circumferential heating-rate distribution; $z/L = 0.95$.

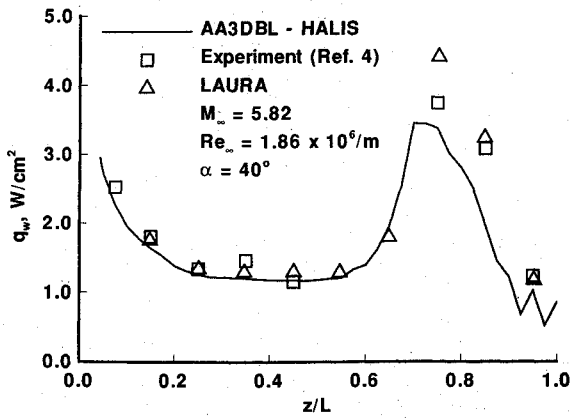

Fig. 14 Heating-rate distribution along leading edge.

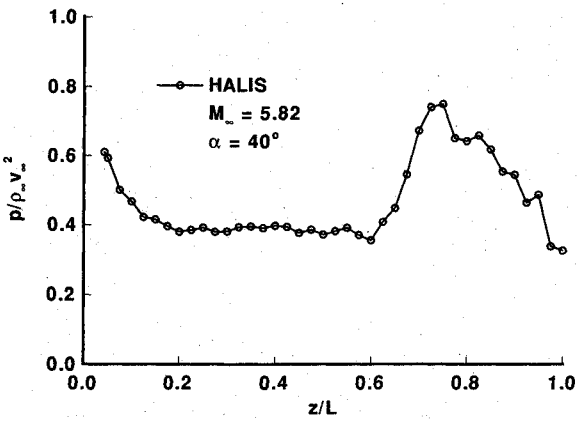

Fig. 15 Pressure distribution along leading edge.

of the body are probably the result of inadequate grid resolution for the HALIS flowfield solution that was discussed previously. The HALIS pressure distribution along the wing leading edge is shown in Fig. 15 where oscillations are noted for $z/L \geq 0.85$. In general, the leading-edge pressure shows similar trends to the heating rate. The computational times for this case are shown in Table 1, but it should be remembered that the run times for the LAURA code could probably be reduced if the code were optimized.

Concluding Remarks

Heating rate calculations have been made on a modified Shuttle Orbiter at a Mach number of 6, a Reynolds number of approximately 1.9 × 10^6/m, and angles of attack of 30 and 40 deg using both a benchmark Navier-Stokes code (LAURA) and an engineering code based on the axisymmetric analog (AA3DBL). The results of these calculations have been compared with experimental data measured in the Langley 20-in. Mach 6 tunnel. Comparisons were made along the windward symmetry plane, in a circumferential direction around the body, and along the wing leading edge. From these comparisons, it has been shown that both the LAURA and AA3DBL codes can be used to accurately predict the heating rate over most of the surface of this Shuttle-like vehicle at large angles of attack. The relatively short run times for AA3DBL make it an ideal engineering code for parametric studies or design.

References

[1]Herrera, B. J., "Results From a Convective Heat Transfer Rate Distribution Test on a 0.0175 Scale Model (22-0) of the Rockwell International Vehicle 4 Space Shuttle Configuration in the AEDC-VKF Tunnel B (OH49B)," Vol. 1, NASA CR-147626, Vol. 2, NASA CR-147627, Oct. 1976.

[2]Hartung, L. C., and Throckmorton, D. A., "Space Shuttle Entry Heating Data Book," Vol. I—STS-2, NASA RP-1191, Vol. II—STS-3, NASA RP-1192, Vol. III—STS-5, NASA RP-1193, May 1988.

[3]Hamilton, H. H., DeJarnette, F. R., and Weilmuenster, K. J., "Application of Axisymmetric Analog for Calculating Heating in Three-Dimensional Flows," *Journal of Spacecraft and Rockets,* Vol. 24, No. 4, 1987, pp. 296–302.

[4]Micol, J., "Aerothermodynamic Measurement and Prediction for a Modified Orbiter at Mach 6 and 10," AIAA Paper 91-1436, June 1991.

[5]Gnoffo, P. A., "An Upwind-Biased, Point-Implicit Relaxation Algorithm for Viscous, Compressible Perfect-Gas Flow," NASA TP-2953, Feb. 1990.

[6]Weilmuenster, K. J., and Hamilton, H. H., "Calculation of Inviscid Flow over Shuttle-Like Vehicles at High Angles of Attack and Comparisons with Experimental Data," NASA TP-2103, May 1983.

[7]Zoby, E. V., Moss, J. N., and Sutton, K. S., "Approximate Convective Heating Equations for Hypersonic Flows," *Journal of Spacecraft and Rockets,* Vol. 18, No. 1, 1981, pp. 64–70.

[8]Roe, P. L., "Approximate Riemann Solvers, Parameter Vectors, and Difference Schemes," *Journal of Computational Physics,* Vol. 43, No. 2, 1981, pp. 357–372.

[9]Yee, H. C., "On Symmetric and Upwind TVD Schemes," NASA TM-86842, Sept. 1985.

[10]Vachris, A. F., and Yaeger L. S., "QUICK-GEOMETRY—A Rapid Response Method for Mathematically Modeling Configuration Geometry," *Applications of Computer Graphics in Engineering,* NASA SP-390, Oct. 1975, pp. 49–73.

Ernest V. Zoby
Associate Editor